# A Comparative Study of Energy-Oriented Driving Strategy for Connected Electric Vehicles on Freeways with Varying Slopes

Bingbing Li [a], Weichao Zhuang [a,*], Hao Zhang [b], Ruixuan Zhao [c], Haoji Liu [a], Linghu Qu [a], Jianrun Zhang [a], Boli Chen [c]

[a] *Department of Mechanical Engineering, Southeast University, Nanjing, 211189, China*
[b] *The State Key Laboratory of Automotive Safety and Energy, Tsinghua University, Beijing 100084, China*
[c] *Department of Electronic and Electrical Engineering, University College London, WC1E 6BT London, U.K.*

***Abstract*—Most eco-driving strategies are developed and tested in simulated environments, neglecting the computational capabilities available on-board, making it challenging to apply them in real-time on actual vehicles. In this paper, two real-time energy-oriented driving strategies are proposed to minimize the energy consumption for electric vehicles (EVs) on highways with varying slopes. First, a novel strategy, called normalized-energy consumption minimization strategy (NCMS), adopts a designed kinetic energy conversion factor to convert the vehicle kinetic energy change into the equivalent battery energy consumption. By minimizing the total normalized energy consumption, the energy-orientated vehicle control sequence is calculated. In addition, a logic car-following algorithm is developed to enhance NCMS for the purpose of avoiding collisions with the potential preceding vehicle on the journey. Second, a driving strategy derived from improvements on existing methods, called improved model predictive control (IMPC) is developed with a hierarchical framework, which achieves a balance between optimization and computational efficiency. In the upper level, a global, coarse-grained, iterative dynamic programming (IDP) is employed to penalize the MPC terminal state, while the lower level performs online rolling optimization of the vehicle within a moderate time step. Thirdly, the performance of the proposed driving strategies is verified through a traffic simulation to evaluate the energy efficiency improvement and processor computation time compared to dynamic programming (DP) and constant speed (CS) strategy. Finally, a vehicle-in-the-loop test is carried out to validate the feasibility of the proposed two novel driving strategies and the reliability of simulation results. Both simulation and real-vehicle experimental results illustrate the significant computational and energy efficiency improvement of the proposed strategy.**

***Index Terms*—Eco-driving, Dynamic programming, Model predictive control, Electric vehicles, Energy efficiency.**

## 1. Introduction

The transportation sector accounts for about 24% of global CO2 emissions [1], thus, governments around the world released increasingly stringent vehicle fuel economy and emission regulations, prompting automakers to develop low-carbon vehicle techniques [2]. Electrification is recognized as an effective way to reduce vehicle carbon emissions [3]. However, the limited charging infrastructure and battery size of electric vehicles (EVs) prevent long-distance travel.

To extend the driving range of EVs, various attempts have been made without increasing battery sizes, including novel vehicle propulsion systems [4]-[7], advanced traffic signal control [8]-[10], and ecological driving. Among them, ecological driving, or called eco-driving, is recognized as a simple and straightforward method to improve vehicle energy efficiency by regulating vehicle longitudinal motion. It can be enabled by training drivers to operate vehicles in an energy-efficient way, i.e., avoiding unnecessary acceleration and idling during the driving process, yet it may increase the operational burden on drivers and labor cost to society [11]-[13]. As an alternative, designing a vehicle longitudinal control system can also minimize vehicle energy consumption through the eco-driving strategy [14]-[21]. Typically, the pulse and Glide (PnG) strategy is recognized as a better energy efficiency performance than constant speed (CS) cruising on flat roads using the optimal control theory [22]. In recent years, emerging information and communication technologies, such as vehicle-to-vehicle (V2V) and vehicle-to-infrastructure (V2I) technologies, have further accelerated the development of eco-driving strategies. Up to now, eco-driving strategy can be divided into two scenarios, i.e., on urban roads with traffic lights and the highways. By contrast, vehicles travelling on the highway, with long driving mileage, are considered to have stronger energy-saving potential by an energy-oriented driving strategy. However, on long-distance highways, various factors such as weather, road gradient, and speed limits can undergo dramatic changes at different spatio-temporal points [23]. These fluctuations necessitate the utilization of a time-varying longitudinal vehicle model, which, in turn, makes achieving global energy optimization for the vehicle more challenging in this situation.

Dynamic programming (DP), a global optimization algorithm, is widely implemented in eco-driving to improve the energy efficiency of vehicles [24]. Based on road slope information, Wang et al. [25] developed an eco-driving strategy using DP. Zhuang et al. [26] employed DP in the cruising speed planning of EVs to realize a tradeoff between energy consumption and degradation of the battery. In addition, Sun et al. [27] developed an optimal speed planning system, based on joint optimization of DP and the interior point method, which was proposed for acquiring the global speed trajectory, achieving remarkably improve energy efficiency by up to 22% in urban driving situations compared with human driving. However, the computation time of DP grows exponentially with

* *Corresponding author.*
*E-mail addresses: wezhuang@seu.edu.cn (W. Zhuang)*

the increase in the number of state and control variables, called the curse of dimensionality, which prevents it from real-time applications in standard microcontrollers. To alleviate the computational effort, various approaches were proposed to develop an eco-driving strategy, including Pontryagin's minimum principle [28], stochastic dynamic programming [29], convex programming [30], as well as model predictive control (MPC) [31]. Among them, MPC, a receding horizon control strategy, is favored for its capacity to adapt to external disturbances and mismatches between the dynamic model and the real system. A hierarchical-level MPC methodology has implemented eco-driving by decoupling vehicle speed planning problems with speed limit constraints [32]. An enhanced MPC was adopted by Zhang et al. in [33] to improve vehicle economy, achieving a 21% energy saving compared with the original control strategy. In addition, a predictive cruise control strategy was proposed for reducing idle time at signalized intersections and fuel consumption using upcoming traffic signal information and utilizing the MPC approach to optimal vehicle speed trajectory prediction, obtaining a 24% energy savings in single-vehicle scenario [34]. Most of these studies directly use the MPC to minimize energy consumption with a non-linear relationship between motor torque and speed, which is a non-linear, non-quadratic, and non-convex problem. Hence, when tackling this issue, a smaller sample time can give rise to an overwhelming computational burden, rendering real-time implementation impractical. Conversely, a longer sample time might yield inadequate energy conservation. To overcome this awkward predicament, various MPC frameworks tracking a "prescribed baseline" to save vehicle energy have been proposed by some academics [35]. The majority of the literature defines a fixed desired velocity as this prescribed baseline [36]-[39], yet a constant desired velocity is not the optimal energy-efficient velocity trajectory for the freeways with varying slopes. Therefore, it is necessary to develop a real-time eco-driving strategy in combination with road slope information.

For this purpose, this paper proposes a novel strategy to achieve real-time energy-oriented driving of connected electric vehicles (CEV) on a highway using terrain information, called normalized energy consumption minimization strategy (NCMS). It is well known that the essence of the PnG strategy is storing the redundant powertrain energy in the type of vehicle kinetic energy and discharging the energy while the vehicle is gliding. Thus, from the view of energy management, the eco-driving strategy is improving energy efficiency by optimizing the energy allocation between battery energy and vehicle kinetic energy. In addition, an improved MPC (IMPC) strategy with a hierarchical architecture is developed based on the most widely applied MPC framework, which achieves a balance between optimization and computational efficiency. Eventually, we compare the proposed strategy with several common existing driving strategies, namely, the globally optimal DP and the widely used CS strategy employed in real-world driving scenarios. The main contributions of this paper are threefold:

(1) A control strategy with high real-time performance, NCMS, is developed in the eco-driving of EVs via transforming vehicle kinetic energy into equivalent battery energy. In comparison to other classical approaches, the designed strategy exhibits comparable enhancements in energy efficiency while demonstrating a remarkable improvement in computational efficiency, which paves the way for novel insights in the realm of eco-driving for EVs.

(2) A logic car-following algorithm is developed to enhance NCMS, which suits both free traffic and car-following scenarios with safety guarantees.

(3) A codesign, IMPC, is implemented in energy-oriented driving of EVs, which incorporates the complementary merits with global optimality of IDP and computational efficiency of MPC. Compared with DP, the implementation of the IDP method yields a substantial enhancement in computational efficiency. By offering penalization at each rolling horizon terminal for MPC, it further ensures energy efficiency within a relatively large time step for the MPC process.

(4) Representative traditional strategy and the designed methods are comprehensively evaluated in a simulated environment and vehicle-in-the-loop test to verify the promising performance of NCMS.

The remainder of this paper is organized as follows. The problem studied in this paper is formulated in Section II. Section III presents the proposed NCMS and IMPC, including the overall architecture of the method, the objective function definition, and physical constraints. Section IV evaluates comparative results for different driving strategies in a simulated environment and vehicle-in-the-loop test. The paper is concluded in Section VI.

## 2. Problem formulation

The concept of energy-oriented driving on a highway with varying slopes is depicted in Fig. 1. This driving strategy not only considers the effects of vehicle dynamics such as frequent acceleration and deceleration on energy consumption but also considers the effect of road gradient. The subject vehicle is a CEV that can obtain the road terrain information using Global Positioning System (GPS) and Geographic Information System (GIS). By optimizing the vehicle speed and powertrain torque coordinately, the operating efficiency of the vehicle powertrain could be improved, and the vehicle energy consumption can be minimized over the whole travelling distance under safety constraints.

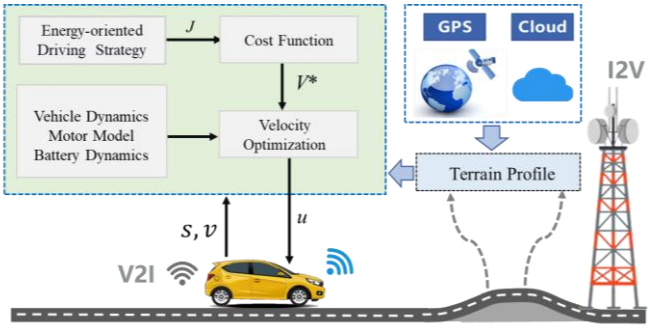


**Fig. 1.** Energy-oriented driving on a highway with varying slopes.

### 2.1 Vehicle model

In this paper, as illustrated in Fig. 2, the study focuses on longitudinal vehicle control, so lateral dynamics are disregarded. The longitudinal acceleration is expressed as

$$a = \frac{T - T_b}{\delta m r} - \frac{g(f\cos(\theta) + \sin(\theta))}{\delta} - \frac{A\rho C_d v^2}{2m\delta} \quad (1)$$

where $a$ is the longitudinal acceleration of the vehicle, $\delta$ is the vehicle rotational inertia coefficient, $m$ is the vehicle mass, $v$ is the vehicle speed, $T$ and $T_b$ are the traction torque and braking torque applied to the tire, respectively. $r$ is the tire rolling radius of the vehicle, $g$ is the gravity constant, $f$, $\theta$, and $C_d$ are the rolling resistance factor, gradient and aerodynamic drag factor, respectively. $A$ is the frontal area, $\rho$ is the air density.

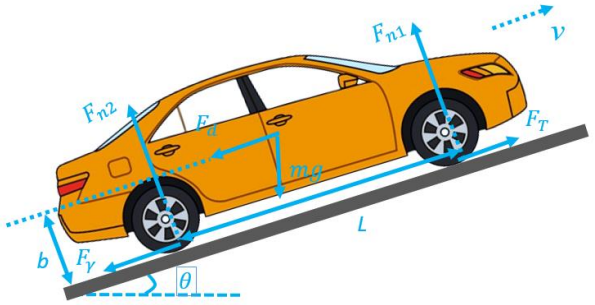


**Fig. 2.** Vehicle longitudinal dynamics on a ramp.

The driving force of the CEV is provided by the motor, and the traction torque and braking torque can be obtained through

$$\begin{cases} T = i_g \eta_t T_{md} & \text{for propulsion} \\ T_b = i_g T_{mb}/\eta_t + T_{fb} & \text{for braking} \end{cases} \quad (2)$$

where $i_g$ is the transmission gear ratio, $\eta_t$ is the transmission efficiency, $T_{md}$ and $T_{mb}$ are the motoring torque and generating torque, respectively. $T_{fb}$ is the mechanical braking torque generated by hydraulic brakes.

### 2.2 Energy consumption model

The characteristics of the motor can typically be obtained from the motor efficiency map provided by the motor manufacturer. In this study, to simplify the model, we mainly establish a quasi-static motor model as shown in Fig. 3, where the motor efficiency is a function of the speed and output torque. The power of the motor can be expressed as

$$P_m = \begin{cases} T_{md}\omega_m/\eta_e & \text{for motoring} \\ T_{mb}\omega_m\eta_e & \text{for generating} \end{cases} \quad (3)$$

with

$$\eta_e = \psi_m(T_{md}, T_{mb}, \omega_m) \quad (4a)$$

$$\omega_m = i_g v/r \quad (4b)$$

where $P_m$ is the motor power, $\eta_e$ is the motor efficiency, $\omega_m$ is the electric motor speed.

### 2.3 Battery model

An equivalent electrical circuit is used to model the lithium-ion phosphate battery system [40], where the complex electrochemical reaction inside the battery is ignored, and only the charge and discharge characteristics of the battery are considered. The battery state-of-charge (SOC) dynamics can be modelled as

$$\dot{\text{SOC}} = -\frac{U_{oc} - \sqrt{U_{oc}^2 - 4R_b P_b}}{2Q_b R_b} \quad (5)$$

with

$$P_b = P_m + P_{aux} \quad (6)$$

where $U_{oc}$ is the open-circuit voltage of the battery, $R_b$ is the internal resistance of the battery, $P_b$ is the terminal battery power, $Q_b$ is the nominal capacity of the battery, $P_{aux}$ is the auxiliary power.

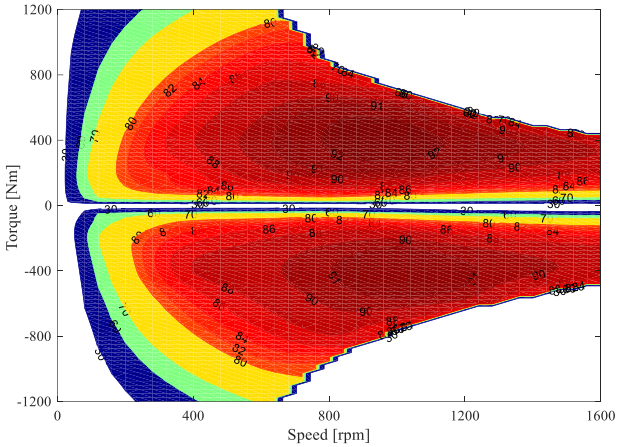


**Fig. 3.** Efficiency map of the motor.

## 3. Energy-oriented driving strategy design

In this section, we present the two real-time energy-oriented driving strategies, i.e., NCMS and IMPC.

### 3.1 Normalized-energy consumption minimization strategy

In the work presented by Li [22], the PnG strategy is introduced, where the internal combustion engine operates in an impulse mode to achieve high fuel efficiency by utilizing the vehicle body as an energy storage. Building upon this concept and considering future applications, the NCMS is proposed as illustrated in Fig. 4, where the kinetic energy of the vehicle body can be regarded as a power source, alongside the battery energy and fuel energy. To better achieve dynamic co-optimization of the two energy sources, this strategy is inspired by the energy management control of hybrid electric vehicles, the equivalent consumption minimization strategy (ECMS). In ECMS, the power distribution strategy between the engine and the electric motor is optimized by minimizing the equivalent consumption, which is composed of transient fuel consumption and electricity consumption [37]. In this paper, the developed NCMS further introduces the concept of ECMS to the speed optimization of EVs. This strategy serves as an instantaneous cruise control method specifically designed for EVs.

The core of the proposed NCMS is to convert the change of vehicle kinetic energy into electric energy consumption through a kinetic energy conversion factor (KECF). The KECF is the weight of the conversion of kinetic energy into electric energy along with different vehicle speeds and road slopes. It should be noted that the higher the vehicle speed, the greater the kinetic energy stored in the vehicle body, and the greater the aerodynamic drag resistance during the vehicle driving. Therefore, to reduce the energy consumption caused by the air

drag resistance and rolling resistance, our proposed NCMS further improves the energy consumption behavior for the same driving time by adjusting the KECF to better utilize the kinetic energy and gravitational potential energy of host vehicle. In other words, it is to reduce the speed of the vehicle to overcome the rolling resistance and air drag resistance, and to convert the kinetic energy of the body to offset the power consumption. On the contrary, when the speed is low, the kinetic energy stored by the vehicle body is low. Currently, it is necessary to increase the weight of kinetic energy conversion (i.e., reducing KECF). Combining the working efficiency of the motor with vehicle power demand, excess motor energy is collected by increasing the kinetic energy reserve, to maintain a higher working efficiency of the motor. The energy consumption of EVs can be equivalently represented as

$$E_{NCMS} = E_e - \beta \Delta E_k \tag{7}$$

with

$$E_e = \int_{t_0}^{t_f} P_b dt \tag{8a}$$

$$\Delta E_k = \int_{t_0}^{t_f} (\frac{1}{2} m v^2 - \frac{1}{2} m v_0^2) dt \tag{8b}$$

where $E_e$ is the electricity consumption, $\Delta E_k$ is the change of vehicle kinetic energy, $\beta$ is the kinetic energy conversion factor (KECF). $t_0$ and $t_f$ are the initial and terminal time, respectively. $v_0$ is the initial velocity. It should be noted that the motor can recover energy by the feedback braking, so $E_e$ may be positive or negative. $E_e < 0$ denotes that the output torque of the motor is negative, and the kinetic energy is converted into electric energy for energy recovery through the feedback braking, and vice versa. Note that kinetic energy can also be converted bidirectionally. $\Delta E_k < 0$ indicates that the vehicle is in a deceleration state when it is desired to transform the kinetic energy of host vehicle to help the motor to do work, aiming to reduce electrical energy consumption. $\Delta E_k > 0$ means that the torque output of the motor exceeds the torque required for constant speed driving, it is necessary to store the kinetic energy of the vehicle and reduce the speed.

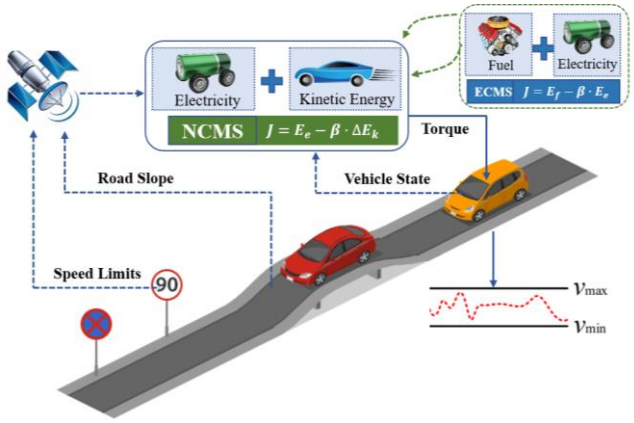


**Fig. 4.** A schematic of the proposed NCMS.

For vehicles traveling long distances, formulating the problem in the spatial domain is more conducive to dealing with the effects of gradient on energy consumption. Consequently, the equivalent energy consumption rate of the vehicle in the spatial domain can be described as

$$P_{NCMS} = \frac{dE_{NCMS}}{ds} = \frac{P_b}{v} - \beta m a \tag{9}$$

Comprehensive analysis of the above, KECF should be related to road gradient and driving speed. In addition, since the value converted from kinetic energy to electrical energy changes dynamically, the specific influence relationship is defined by the numerical tests as follows

$$\beta = \varepsilon \cdot \frac{\varphi(\theta)}{\varphi(\theta) + C_d \cdot \mu_m} \tag{10}$$

where

$$\mu_m = \frac{v^2 - 0.5(v_{max}^2 + v_{min}^2)}{v_{max}^2 - v_{min}^2} \tag{11}$$

where $\varepsilon$ denotes the displacement coefficient of vehicle kinetic energy converted into battery power, $\varphi(\theta)$ is the road resistance of the vehicle including the gradient and rolling resistance, i.e., $\varphi(\theta) = mgsin(\theta) + mgfcos(\theta)$. Since the kinetic energy of the vehicle body is regarded as configurable driving energy, the cruising speed will fluctuate up and down within the set speed range, $v_{max}$ and $v_{min}$ are the maximum and minimum vehicle speeds in the cruising speed range, respectively, i.e., upper and lower bounds of road speed limits

To specifically observe the relationship between the change of KECF and the road gradient and driving speed, the analysis in Fig. 5 is done based on Eq. (10), where $\beta$ is calculated under the different road gradient (0°~10°) and driving speed (13 m/s-21 m/s). As shown in Fig. 5, when the vehicle speed is high, the weight of kinetic energy is less than 1. As the vehicle speed decreases, the weight of kinetic energy is greater than 1. Moreover, the size of the road gradient exacerbates this relationship. With the decrease of the road slope, the gradient resistance gradually reduces its impact on vehicle kinetic energy, and it is obvious that the influence of vehicle speed on KECF is greater relative to the slope.

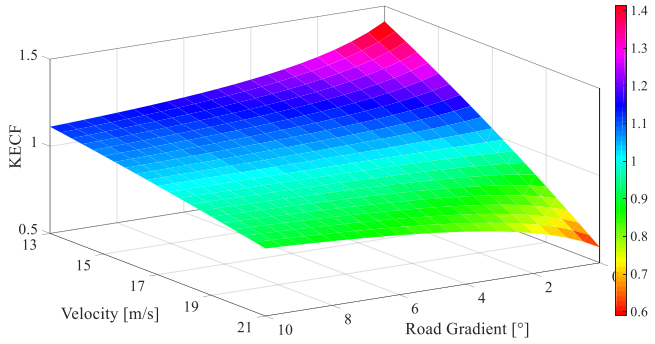


**Fig. 5.** The range of KECF $\beta$.

To implement the NCMS with a dynamics model, an optimal problem is formulated. An objective function is minimized and expressed as

$$\min_u J = \int_{s_0}^{s_f} P_{NCMS}(T, T_b, t, v) ds \tag{12}$$

subject to (2)-(11) and

$$\frac{dv}{ds}=\begin{bmatrix}\frac{dt}{ds}\\ \frac{dv}{ds}\end{bmatrix}=\begin{bmatrix}\frac{1}{v}\\ \frac{T-T_b}{\delta mrv}-\frac{g(f\cos(\theta)+\sin(\theta))}{\delta v}-\frac{A\rho C_d v}{2m\delta}\end{bmatrix} \quad (13a)$$

$$v_{min}\le v(s)\le v_{max} \quad (13b)$$

$$T_{md,min}(\omega_m)\le T_{md}(s)\le T_{md,max}(\omega_m) \quad (13c)$$

$$\omega_{m,min}\le \omega_m(s)\le \omega_{m,max} \quad (13d)$$

$$T_{mb}\le T_{mb,min} \quad (13e)$$

$$|\dot{a}|\le j_{max} \quad (13f)$$

where $s_0$ and $s_f$ are the start and end position of the journey, respectively. $s$ is the vehicle position $x=[t,v]^{\mathrm{T}}$ is the state variable including travel time $t$ and speed $v$, $u=[T,T_b]^{\mathrm{T}}$ is the control variable including traction torque $T$ and braking torque $T_b$. $\dot{a}$ is the accelerated derivative, $j_{max}$ is the maximum accelerated derivative.

In pursuit of computational efficiency, we introduce a rolling distance-domain method (RDM) rather than a full horizon optimization. This innovative approach focuses on solving control sequences within a limited forward distance during each horizon *H*, as shown in Fig. 6. The entire journey is divided into *n* stages, i.e., $s_f-s_0=\sum_{k=1}^{n}H_k$. For any of these stages *k*, the end state of the previous stage *k*-1 is used as the initial state of the current stage *k*, while the end state of the current stage *k* will serve as the initial state of the next stage *k*+1. In this way, the vehicle can derive the optimal state sequence $x_{op,k}$ and control sequence $u_{op,k}$ for each stage. Eventually, the optimal state sequence $[x_{op,1},\ x_{op,2},\ \cdots,x_{op,n}]$ and the control input sequence $[u_{op,1},u_{op,2},\cdots,u_{op,n}]$ for the whole journey are obtained.

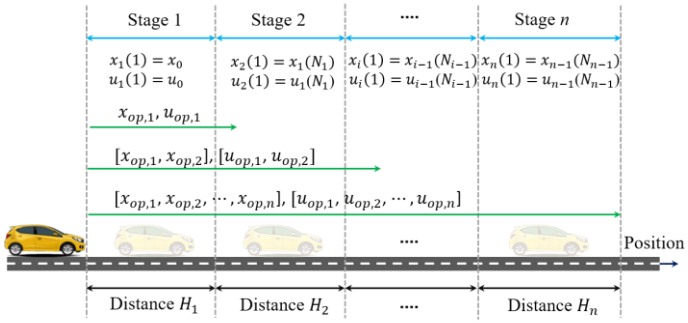


**Fig. 6.** Schematic diagram of RDM**.**

In each distance horizon, the optimal control problem is formulated as follows

$$\min J=\sum_{i=1}^{N}P_{NCMS}(T,T_b,t,v)\Delta s \quad (14)$$

subject to

$$\begin{cases}v(i+1)=\sqrt{v(i)^2+2a(i)\Delta s}\\ t(i+1)=t(i)+\dfrac{\Delta s}{\overline{v}(i)}\end{cases} \quad (15a)$$

$$v_{min}\le v(i)\le v_{max} \quad (15b)$$

$$T_{md,min}(\omega_m)\le T_{md}(i)\le T_{md,max}(\omega_m) \quad (15c)$$

$$\omega_{m,min}\le \omega_m(i)\le \omega_{m,max} \quad (15d)$$

$$T_{mb}(i)\le T_{mb,min} \quad (15e)$$

$$|a(i)-a(i-1)|\le j_{max} \quad (15f)$$

where $\Delta s$ is the sampling distance. $\overline{v}(i)$ is the average speed in $i$th distance step, i.e., $\overline{v}(i)=0.5(v(i)+v(i+1))$. N is the number of distance steps in each stage, i.e., $N=H/\Delta s+1$.

### *3.2 Controller design for NCMS in car-following scenarios*

The behavior of the host vehicle may be constrained by the vehicle in front during long-distance travel, so the safety of the host vehicle must be ensured. In this section, a logic car-following algorithm is designed for both control strategies. The detailed logic car-following algorithm is further presented in Fig. 7. The incorporation of driving safety constraints necessitates the host vehicle to adhere to a maximum safe acceleration limit upon detecting a vehicle ahead via radar, thereby avoiding potential collisions. For this purpose, the Gipps model is adopted as the longitudinal car-following model in this study. The Gipps model follows a deterministic acceleration modelling framework and proves to be well-suited for characterizing vehicles equipped with adaptive cruise control, facilitating platoon formation. It is important to note that other car-following models specifically designed for connected vehicle systems could be considered as alternatives to the Gipps model in the proposed framework. The Gipps formulates the predicted acceleration rate as

$$\begin{aligned}&v(t+\Delta t)\\ &=b\Delta t\\ &+\sqrt{b^2\Delta t^2-2b(\Delta s-d_0)+bv(t)\Delta t+bv_p^2/b_p}\end{aligned} \quad (16)$$

with

$$\Delta s=s_p-s \quad (17)$$

where $b$ and $b_p$ denote the maximum braking deceleration of the host vehicle and preceding vehicle, respectively. $v_p$ and $s_p$ are the speed and position of the preceding vehicle, respectively. $d_0$ is the static inter-vehicle distance, $\Delta t$ is the response time of the braking system, $\Delta s$ is the inter-vehicle distance between the host vehicle and the preceding vehicle. The parameters of the Gipps are summarized in Table 2.

**Table 1**
Parameters of Gipps

| Parameter | Value | Parameter | Value |
|---|---|---|---|
| $b$ | -6 m/s$^2$ | $\Delta t$ | 0.55 s |
| $b_p$ | -6 m/s$^2$ | $d_0$ | 4.5 m |

In the following scenario, we assume that the host vehicle with adaptive cruise capability can monitor the surrounding vehicles or obstacles with the help of millimeter-wave radar. In Fig. 7, when there are no vehicles detected within the radar detection range *D* of the host vehicle, it follows the ecological acceleration $a_e$ planned by the proposed NCMS. However, when there is a leading vehicle within *D*, the host vehicle will choose the smaller acceleration between $a_e$ and safety acceleration $a_s$ as its input to achieve a trade-off between vehicle safety and driving economy. Here safety acceleration $a_s$ can be obtained by the Gipps model, i.e.

$$a_s(t)=\frac{v(t+\Delta t)-v(t)}{\Delta t} \quad (18)$$

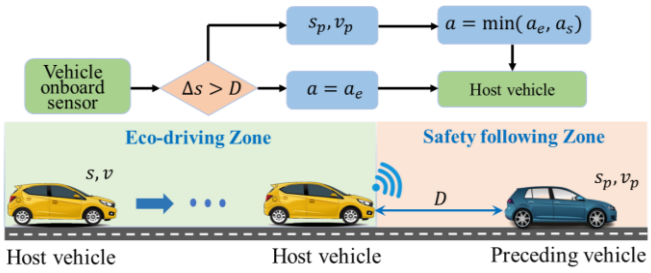


**Fig. 7.** Flow diagram of the logic car-following algorithm.

### *3.3 Improved model predictive control strategy*

To demonstrate the algorithmic efficiency and energy efficiency improvement of NCMS, this section presents a novel IMPC strategy designed for real-time driving control of an EV. This strategy strikes a balance between the global optimality offered by IDP and the real-time performance of MPC, thereby overcoming the challenge of MPC getting trapped in local optimality. In addition, the utilization of the IDP technique leads to improved computational efficiency in contrast to the traditional offline DP method. This enhancement is attained through a two-step iterative strategy that involves the systematic scaling of state and control variables grids. The presented IMPC, as shown in Fig. 8, employs a bi-level framework. In this approach, the upper level computes an optimized trajectory sequence based on a coarse discretization of state variables using IDP, and the lower level refines the IDP output in a smaller time step based on the MPC.

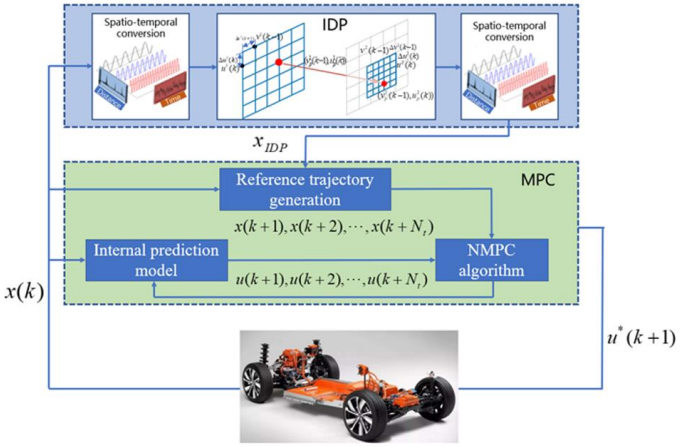


**Fig. 8.** A schematic representation of the IMPC strategy.

Within the bi-level framework, the upper-level IDP algorithm, resulting in a global solution, focuses on the minimization of energy consumption. To effectively address this issue, IDP operates in a backward manner similar to RDM. By discretizing the distance, it ensures an equitable comparison of power consumption within each segment. The algorithm optimizes control inputs at each distance step to ascertain the most efficient energy consumption, progressively working towards the destination. Ultimately, IDP generates an optimal state sequence that maximizes performance while minimizing energy usage.

Therefore, each stage is divided into $N_{IDP}$ parts by the distance step $\Delta s_{IDP}$, instead of discretizing the problem in the time domain, the cost function of the optimization problem is

$$\min J = \sum_{i=1}^{N_{IDP}} \Delta SOC\left(T(i), T_b(i), v(i)\right) \frac{\Delta s_{IDP}}{\overline{v}(i)} \tag{19}$$

subject to

$$\begin{cases} s(i+1) = s(i) + \Delta s_{IDP} \\ v(i+1) = \sqrt{v(i)^2 + 2a(i)\Delta s_{IDP}} \end{cases} \tag{20a}$$

$$v_{min} \le v(i) \le v_{max} \tag{20b}$$

$$T_{md,min}(\omega_m) \le T_{md}(i) \le T_{md,max}(\omega_m) \tag{20c}$$

$$\omega_{m,min} \le \omega_m(i) \le \omega_{m,max} \tag{20d}$$

$$T_{mb}(i) \le T_{mb,min} \tag{20e}$$

$$|a(i+1) - a(i)| \le j_{max} \tag{20f}$$

The IDP algorithm is a two-step iterative approach that refines the state and control variable grids based on DP, which aims to improve computational efficiency by reducing mesh density. In the first iteration, the initial state variable boundaries $[x^1_{min}, x^1_{max}]$, control variable boundaries $[u^1_{min}, u^1_{max}]$ and the initial grid sizes $\Delta x^1$ and $\Delta u^1$ are input, and the optimal state variable $x_{op}$ and optimal control variable $u_{op}$ are calculated according to the DP algorithm. Then, the second iteration of IDP is shown in the Eq. (21)-(24), where $[x^1_{min}, x^1_{max}]$ and $[u^1_{min}, u^1_{max}]$ are updated based on the boundary of the optimal result obtained in the first iteration, i.e. $[x^1_{op,min}, x^1_{op,max}]$ and $[u^1_{op,min}, u^1_{op,max}]$. This update helps refine the grids and focus on regions of interest. To prevent state points from falling at the boundaries of the grid, the state and control variables scaling factors $\sigma$ and $\tau$ are introduced to reasonably adjust the boundary range. The adjustments ensure that state and control points are placed away from the edges, providing a more stable and accurate representation of the problem. Therefore, with enough iterations, IDP will be able to achieve the same optimization effect as DP.

$$x^2_{max} = \min\left(x^1_{op,max} - \sigma \cdot \Delta x^1, x_{max}\right) \tag{21}$$

$$x^2_{min} = \max\left(x^1_{op,min} + \sigma \cdot \Delta x^1, x_{min}\right) \tag{22}$$

$$u^2_{max} = \min\left(u^1_{op,max} - \tau \cdot \Delta u^1, u_{max}\right) \tag{23}$$

$$u^2_{min} = \max\left(u^1_{op,min} + \tau \cdot \Delta u^1, u_{max}\right) \tag{24}$$

In the second iteration, the mesh sizes $\Delta x^2$ and $\Delta u^2$ are also updated by the shrinking factors $\xi$ and $\gamma$ as follows

$$\Delta x^2 = \xi \cdot \Delta x \tag{25}$$

$$\Delta u^2 = \gamma \cdot \Delta u \tag{26}$$

where $\xi$ and $\gamma$ affect the grid density. Thus, the hyperparameter $\boldsymbol{\pi} = [\Delta x, \Delta u, \sigma, \tau, \xi, \gamma]$ in the IDP algorithm is crucial in balancing algorithm efficiency and optimization performance, which are summarized in Table 2. Since MPC is a time-domain control strategy and IDP is solved discrete in the distance domain, ultimately, the optimized state sequence of IDP after the transformation of time and space domains is shown in Eq. (27)-(28). For any stage $k$, these results are referenced by the lower MPC to make control decisions.

**Table 2**
Parameters of IDP

| Parameter | Range of value | Parameter | Range of value |
|---|---|---|---|
| $\Delta v$ | [0.3 m/s, 3 m/s] | $\tau$ | [0, 1] |
| $\Delta u$ | [10 Nm, 500 Nm] | $\xi$ | [0.1, 1] |
| $\sigma$ | [0, 1] | $\gamma$ | [0.01, 1] |

$$v_{op,k} = [v_k(1), v_k(2), \cdots, v_k(N_{IDP})] \quad (27)$$
$$s_{op,k} = [s_k(1), s_k(2), \cdots, s_k(N_{IDP})] \quad (28)$$

In the lower layer, the coarsely gridded IDP solution is employed to formulate penalties on the terminal states $(s_{f,des}, v_{f,des})$ during the MPC optimization process. Additionally, it serves as the initial guess for the sequential quadratic programming (SQP) solver. The cost function of the IMPC over each prediction horizon is expressed as

$$\begin{aligned} \min J = & \sum_{i=k}^{k+N_m-1} \Delta SOC(T(k), T_b(k), v(k))\Delta t_{mpc} \\ & + w_1 \left(\min\left(0, s(k+N_m|k) - s_{f,des}\right)\right)^2 \\ & + w_2 \left(\min\left(0, v(k+N_m|k)\right.\right. \\ & \left.\left. - v_{f,des}\right)\right)^2 \end{aligned} \quad (29)$$

subject to

$$\begin{cases} s(i+1|k) = s(i|k) + \dfrac{(v(i+1|k) + v(i|k))\Delta t_{mpc}}{2} \\ v(i+1|k) = v(i|k) + a(i|k)\Delta t_{mpc} \end{cases} \quad (30a)$$
$$v_{min} \le v(i|k) \le v_{max} \quad (30b)$$
$$T_{md,min}(\omega_m) \le T_{md}(i|k) \le T_{md,max}(\omega_m) \quad (30c)$$
$$\omega_{m,min} \le \omega_m(i|k) \le \omega_{m,max} \quad (30d)$$
$$T_{mb}(i|k) \le T_{mb,min} \quad (30e)$$
$$|a(i+1|k) - a(i|k)| \le j_{max} \quad (30f)$$

where $(i|k)$ represents the corresponding value of a variable at step $i$ predicted at time $k$, $N_m$ is the prediction horizon of the MPC, $\Delta t_{mpc}$ is the time step used by the MPC, $w_1$ and $w_2$ denote tunable weights to regulate the relative importance of the target terminal position $s_{f,des}$ and velocity $v_{f,des}$ transmitted down from the upper-level IDP.

## 4. Simulations and results

To validate the performance of the proposed candidate driving strategies, a series of simulations are performed in a workstation with Intel® Core™ i7-10875H CPU @ 2.3 GHz and 16 GB RAM. Furthermore, a vehicle-in-the-loop experiment of the prototype CEV is conducted in a real-world road, where the CEV interacts with the environment in real time.

### *4.1 Given route and simulation setup*

In the simulation, a specific highway route, Zhigu Avenue, located in Nanjing City, China, is carefully selected, as illustrated in Fig. 9. This chosen route spans approximately 35 km and traverses the scenic foothills of Zhongshan and Jiuhua Mountain. To acquire the road elevation information for the experimental route, data packets from the designated section on the map are extracted by Google Maps. However, the collected data may contain rough singularities arising from sensor accuracy, signal interference, and other influencing factors. To address this issue, a five-point triple smoothing method is employed to effectively mitigate irregularities and singularities in the data, resulting in a smoothed road elevation profile, as depicted in Fig. 10. Notably, the smoothed profile shows a series of distinct ascending and descending slopes. The main parameters of the simulated vehicle are shown in Table 3, and Table 4 demonstrates the parameter settings of the proposed algorithm.

Apart from conducting a comparative analysis between the two proposed strategies, we also compared them with two common driving strategies: DP and CS strategy. To increase the fairness of the comparison, the speed of CS is set to the average speed obtained by DP.

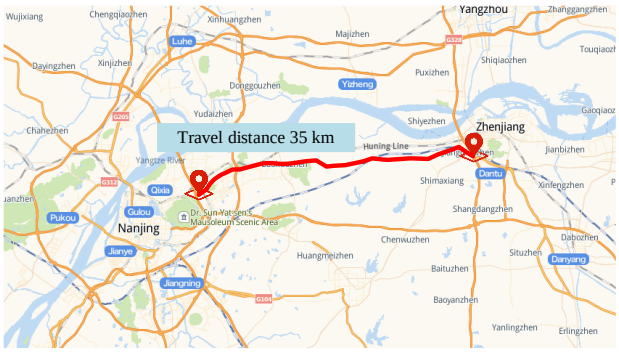


**Fig. 9.** The experimental route in Nanjing City, China.

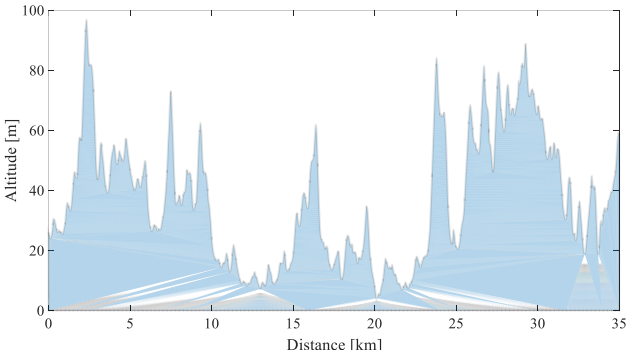


**Fig. 10.** The road elevation of the experimental route obtained from digital road maps.

**Table 3**
Parameters of the subject vehicle

| Component | Parameter | Symbol | Value |
|---|---|---|---|
| Vehicle | Mass | $m$ | 2500 kg |
| | Accessory power | $P_{aux}$ | 400 W |
| | Tire radius | $r$ | 0.36 m |
| | Transmission efficiency | $\eta_t$ | 0.95 |
| | Transmission gear ratio | $i_g$ | 1 |
| | Frontal area | $A$ | 2.45 m$^2$ |
| | Air drag resistance coefficient | $C_d$ | 0.28 |
| | Rolling resistance coefficient | $f$ | 0.015 |
| | Air density | $\rho$ | 1.202kg/m$^3$ |
| | Gravity factor | $g$ | 9.81 m/s$^2$ |
| Motor | Maximum motoring torque | $T_{m,max}$ | 1225 Nm |
| | Minimum generating torque | $T_{mb,min}$ | -1225 Nm |
| | Maximum Speed | $\omega_{max}$ | 1600 rpm |
| Battery | Open-circuit voltage | $U_{oc}$ | 365 V |
| | Charge/discharge internal resistance | $R_b$ | 0.032/0.029Ω |
| | Nominal capacity | $Q_b$ | 48 kWh |

**Table 4**
Algorithm parameters

| Parameter | Symbol | Value |
|---|---|---|
| Sampling distance of NCMS | $\Delta s$ | 1 m |
| Predictive distance horizon | $H$ | 400 m |
| Minimum speed | $v_{min}$ | 13.89 m/s (50 km/h) |
| Maximum speed | $v_{max}$ | 20 m/s |
| Maximum accelerated derivative | $j_{max}$ | 2 m/s$^3$ |
| Sampling distance of IDP | $\Delta s_{IDP}$ | 10 m |
| Sampling time of MPC | $\Delta t_{mpc}$ | 0.1 s |
| Radar detection range | $D$ | 50 m |
| Initial speed | $v_0$ | 16.67 m/s (60 km/h) |
| Initial SOC | $SOC_0$ | 80% |

### *4.2 Simulation results*

Fig. 11 shows the simulation results of vehicle velocity trajectories for different driving strategies along the experimental route. It can be seen that the vehicle velocity trajectories of the IMPC are very close to that of the DP algorithm and lower than that of the NCMS. Table 5 further compares their overall difference in speed, the average speed of the three strategies was calculated, where the average speed of the NCMS reached 16.58 m/s, followed by DP and IMPC with 15.5 m/s and 15.25 m/s, respectively. Therefore, the NCMS consumed the least amount of time for the whole journey.

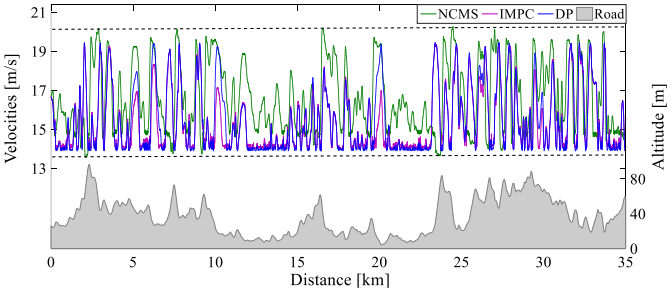


**Fig. 11.** A comparison of vehicle velocity trajectories for different strategies along the experimental route.

In order to compare the characteristics of the different driving strategies, we analyze the speed change characteristics of the four driving strategies in detail below:

For the DP method, the vehicle speed trajectory exhibits an irregular trend in response to changes in road curvature, as depicted in Fig. 12. On relatively flat road sections, the speed is maintained at 13.89 m/s with minimal fluctuations, which aligns with the motor's lowest electricity consumption. This finding further confirms that avoiding unnecessary acceleration and deceleration to maintain a constant speed leads to a significant reduction in energy consumption. However, in areas with significant changes in gradient, such as the road terrain marked in red in Fig. 12, the speed undergoes dramatic variations, transitioning between uphill and downhill stretches. At the lowest elevation point of the road, the vehicle reaches its maximum speed, and vice versa. It is evident that adjusting the speed in accordance with the changes in road terrain proves to be effective in reducing energy consumption.

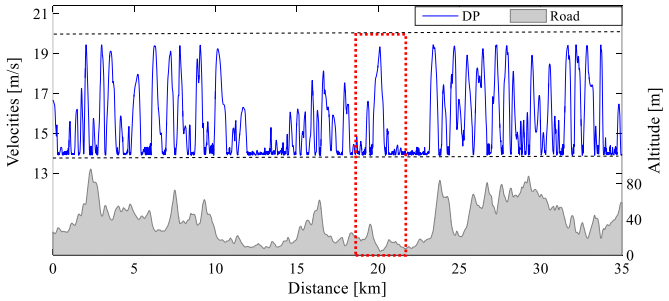


**Fig. 12.** Vehicle velocity trajectories of DP with corresponding road slope.

Fig. 13 demonstrates that the speeds generated by the IMPC and DP generally align with each other, indicating that speed planning based on local road gradient information can yield favorable results. Fig. 14 compares the SOC variations of IMPC and DP, further validating the similarity of the two driving strategies. However, there are certain locations, such as those marked at 5 km, 10 km, and 20 km in Fig. 14, where the IMPC fails to achieve optimal speed planning in comparison to the DP. To conduct a more detailed comparison of the speed differences between the two control strategies, we zoomed in on the speed profile near the 20 km mark and correlated it with the terrain shown in Fig. 15. Notably, the speed profile obtained by the DP exhibits significantly higher magnitude changes. The reason for this difference lies in the fact that the IMPC experiences a delay of approximately 100 m in initiating speed increments. It determines that the vehicle is traversing a downhill slope, and hence utilizes feedback braking to recover energy. Subsequently, when the vehicle encounters a transition from the downhill to a smooth road ahead, it increases its speed and stores energy to mitigate efficiency losses arising from the motor operation. Conversely, the DP is based on global planning, anticipates future road changes, and can plan vehicle speed considering the complete road information available. This difference in approach accounts for the variations in speed planning results between the IMPC and DP at specific locations, highlighting the importance of real-time decision-making and the utilization of comprehensive road data in achieving optimal speed trajectories.

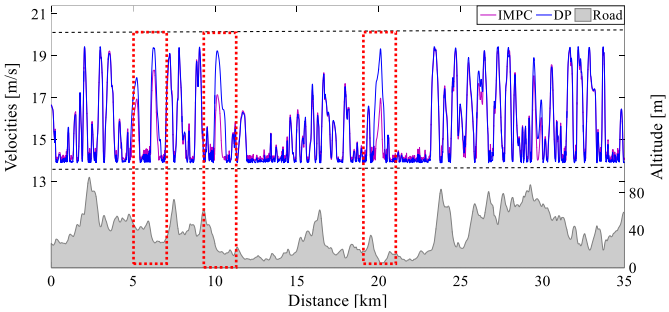


**Fig. 13.** A comparison of vehicle velocity trajectories between the DP and IMPC.

**Table 5**
Comparison of the results of different strategies.

| Driving strategies | Average speed | Final SOC | Change of SOC | Energy saving | Calculation time per step |
|---|---|---|---|---|---|
| CS | 15.5 m/s | 66.26 | 13.74 | -- | -- |
| DP | 15.5 m/s | 68.08 | 11.92 | 13.25% | -- |
| IMPC | 15.25 m/s | 67.86 | 12.14 | 11.64% | 0.35 s |
| NCMS | 16.58 m/s | 67.39 | 12.61 | 8.23% | 0.02 s |

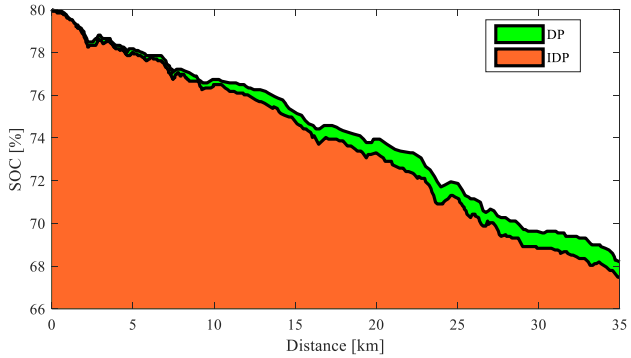


**Fig. 14.** Comparison of SOC changes between IMPC and DP.

To illustrate the performance of the IDP, we compared the velocity trajectories of the DP and IDP planning over the 800 m journey. In Fig. 16, it can be seen that as the number of IDP iterations increases, the speed of IDP is gradually close to that of DP, especially the speed of IDP is basically coincident with that of DP after 10 iterations. Fig. 16 illustrates the computation time of DP versus IDP with different numbers of iterations. Although the computation time of IDP increases with the number of iterations, it is significantly more efficient with respect to DP.

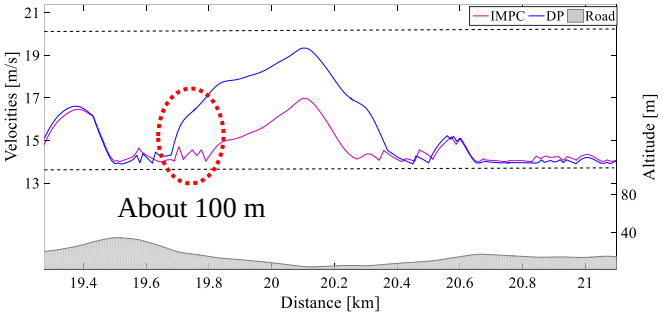


**Fig. 15.** Analysis of speed difference around 20 km of the experimental road.

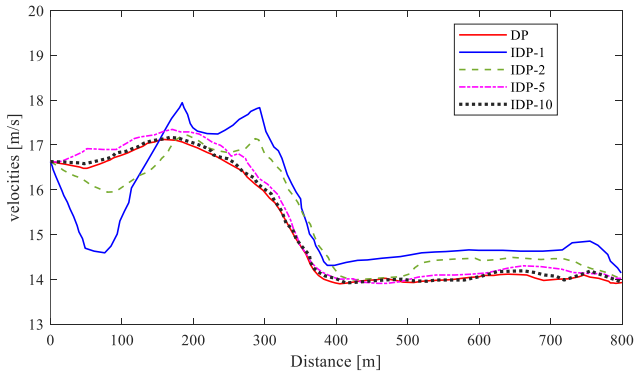


**Fig. 16.** Comparison of the speed of IDP and DP.

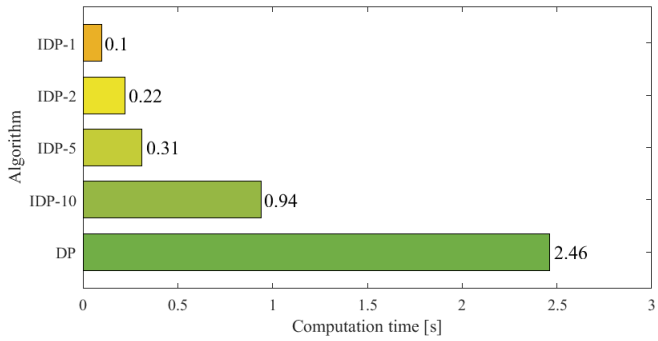


**Fig. 17.** Comparison of computation time of DP and IDP.

For the NCMS driving strategy, as can be seen in Fig. 11 that the vehicle speed is well-restricted within a predetermined range, which varies with the road gradient. In road sections with gentle slopes, the vehicle's speed variation range is relatively stable and consistently maintained at a lower speed level. This deliberate control of speed aims to minimize energy consumption associated with overcoming air resistance, as lower speeds require less power to counteract aerodynamic drag. Conversely, on uphill and downhill sections with steeper gradients, the variation in vehicle speed becomes more pronounced. In such situations, additional measures are taken to optimize energy efficiency. The motor actively assists by strategically managing the kinetic energy conversion of the vehicle. This approach helps to mitigate energy losses due to the efficiency characteristics of the motor, ultimately leading to more effective energy utilization. The speed adjustment of the NCMS is achieved through the implementation of the KECF, as illustrated in Fig. 18. The KECF dynamically adapts the proportional distribution of vehicle kinetic energy based on the road gradient.

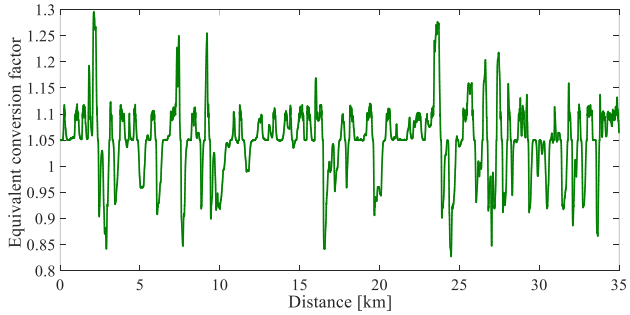


**Fig. 18.** The range of KECF along the experimental route.

To illustrate the energy efficiency benefits of the speed variation, we compared the motor operating points of NCMS and CS. Fig. 19 demonstrates that NCMS exhibits larger driving torque outputs in the low-speed range, with a tendency to approach the high-efficiency region. It is noteworthy that

NCMS shows torque discontinuities in the range of 100 Nm to 350 Nm, as these torque levels correspond to relatively lower motor power efficiency. On the other hand, for CS, the motor operates at a constant speed, resulting in a vertical line distribution in Fig. 19.

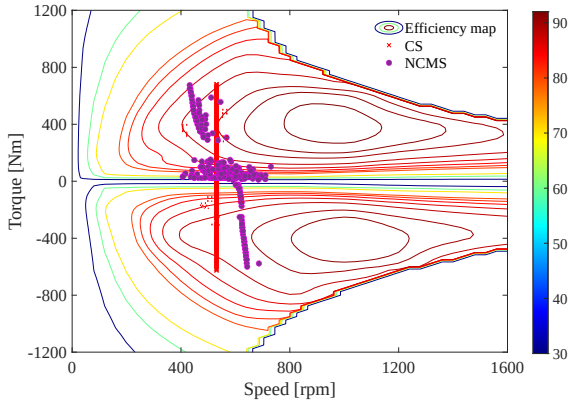


**Fig. 19.** Operating points of the motor for CS and NCMS.

For an unbiased comparison among the different driving strategies, a comparison of motor torque is shown in Fig. 20. The differences in motor operation characteristics between the three energy-oriented driving strategies and CS are as follows:

(1) The peak output torque of the motor is reduced, and the frequency of the motor operating at high torque levels is significantly decreased.

(2) The instances of motor feedback braking are notably reduced. While vehicle feedback braking allows for energy recovery, it also leads to inevitable energy loss due to efficiency losses.

(3) The motor operates more frequently at the zero-output torque point, during which the vehicle is in a coasting state with no power input.

Just like Fig. 19, Fig. 20(c) demonstrates that NCMS significantly improves the motor operating efficiency by adjusting kinetic energy conversion. In Fig. 20(c), the frequency of motor feedback braking is significantly reduced. Within the driving working range, the motor predominantly operates under low-torque conditions. When facing high torque demands, the motor is selectively operated at approximately 400 Nm, which aligns with the outcomes obtained through simulation using DP optimization. The observed intermittent nature of the motor operation, characterized by transitions from low to high torque, may indicate a potential pursuit of higher work efficiency. Regarding the IMPC strategy, it is evident that the strategy applies high torque braking at specific distances, such as 5 km, 10 km, and 20 km, consistent with the vehicle trajectory presented in Fig. 13. The difference between the velocity trajectories of DP and IMPC and the motor output torque could be attributed to the limitations of MPC. The effectiveness of MPC is bounded by the prediction horizon, making it more prone to local optimum solutions.

The quantitative outcomes of the four driving strategies (DP, IMPC, NCMS, CS) are summarized in Table 5. The DP leads to the smallest total cost, followed by the IMPC, and then the NCMS and CS method. It is discernible that the DP consumes less energy than the other three strategies, saving 13.25% compared to CS, thanks to the fact that DP is a global optimization, yet its computation time is also a tremendous challenge. Compared to the DP, the IMPC energy savings is a comparable 11.64%, while the calculation time for a single step is 0.35 s. Specifically, the energy savings of the NCMS is 8.23%, and the calculation time is 0.02 s, which is faster than the IMPC, further indicating that the NCMS has the advantages of low computation burden and high real-time performance, with significant practical significance for future optimization calculation of real vehicles.

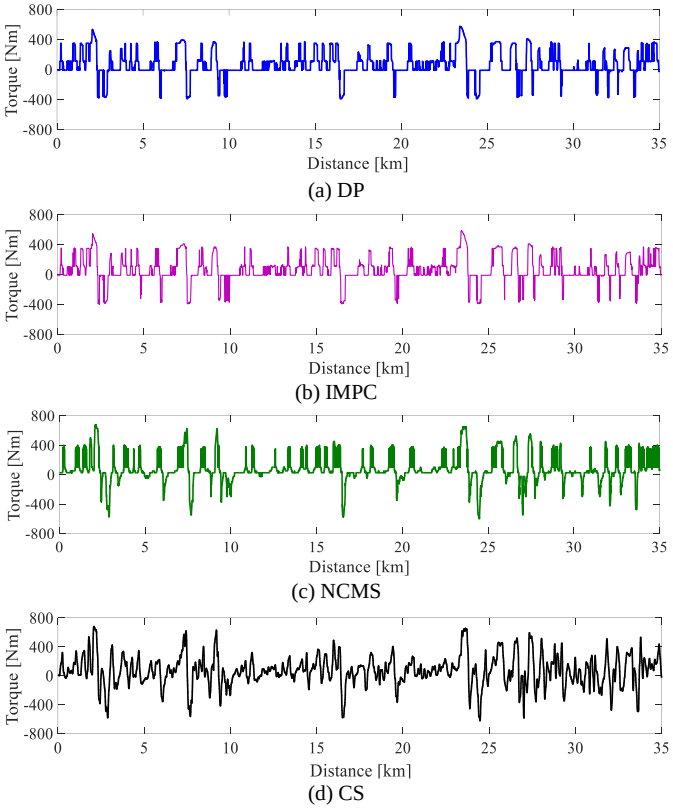


**Fig. 20.** The motor torque of different strategies.

To verify the effectiveness of the proposed logic car-following algorithm, we simulate a car-following scenario. The logic car-following algorithm of NCMS under collision avoidance constraints is verified under the 4 km road scenario, as shown in right half of Fig. 24. This road is taken from a suburban highway near Laoshan in Nanjing, China. We set that the initial speed of the host vehicle is 17 m/s. At 150 m along the road, there is a preceding vehicle cruising at 15.5 m/s and slowly accelerating to 16 m/s at 2 km and maintaining the speed.

Fig. 21 to Fig. 23 show the acceleration, velocity, and following distance of the NCMS in the car-following scenario with the logic car-following algorithm. It is evident that after the preceding vehicle enters the radar detection area of the host vehicle, the following acceleration of the host vehicle is dynamically adjusted between $a_e$ and $a_s$, enabling the host vehicle to effectively avoid the occurrence of rear-end collisions. During the whole journey, the ecological vehicle velocity is not strictly followed by the host vehicle due to the rear-end collision avoidance constraints. However, the host

vehicle was able to maintain a safe distance from the preceding vehicle, which effectively confirms that NCMS is a practical and safe driving strategy. This approach can simultaneously meet the demands of economy, safety, and real-time driving, making it highly practical and promising for future applications.

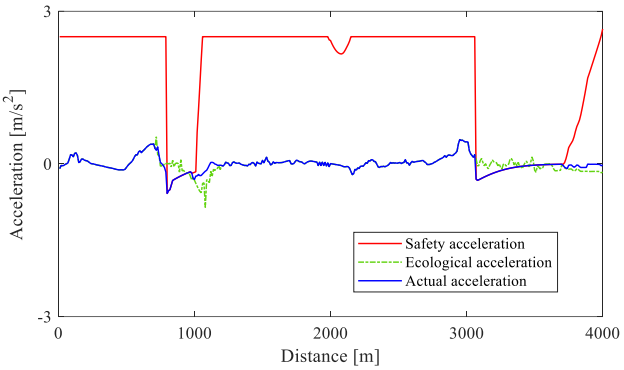


**Fig. 21.** Acceleration of NCMS in the car-following scenario.

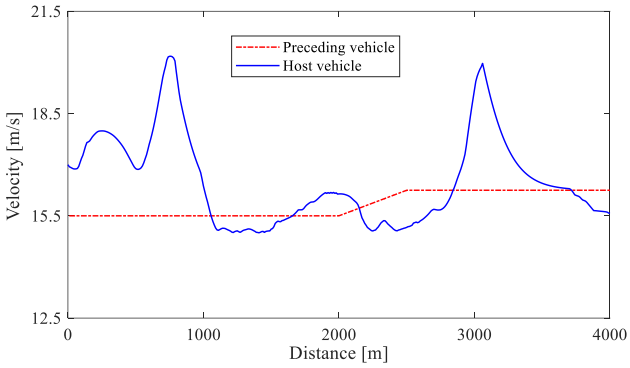


**Fig. 22.** Velocity of NCMS in the car-following scenario.

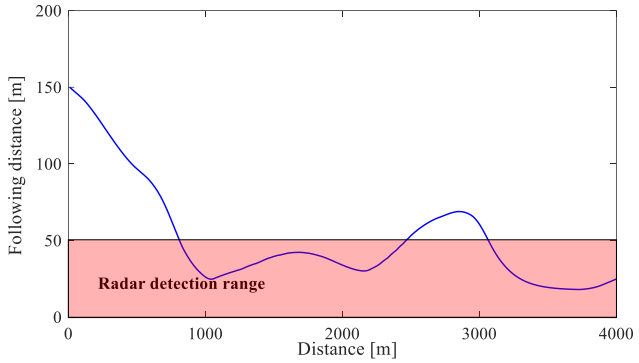


**Fig. 23.** Following distance of NCMS in the car-following scenario.

### *4.3 Vehicle-in-the-loop test*

The experimental vehicle is a modified Chery Ant, equipped with autonomous driving capabilities as shown in Fig. 24. The vehicle mainly consists of two parts: hardware and software. The hardware part includes four modules, namely the perception module, the communication module, the positioning module, and the computing module. For perception, a Bosch camera, a Delphi millimeter-wave radar, and a Hesai LIDAR are used to provide the vehicle with essential environmental information about its surroundings. The communication module is a mobile workstation equipped with an Intel Core i7-7700 @ 3.6 GHz CPU and 16GB of memory. The vehicle's positioning primarily relies on a NovAtel GNSS/INS system. The communication between the mobile workstation and the sensors takes place over Ethernet, facilitated by a Cisco 3560 network switch. Regarding the vehicle software, it utilizes the ROS network for socket-based communication, enabling interactions with microsimulation, sensor fusion, advanced motion planning, and low-level drive control modules. In this study, the low-level controllers run at a frequency of 35 Hz on the mobile workstation, whereas the high-level controllers

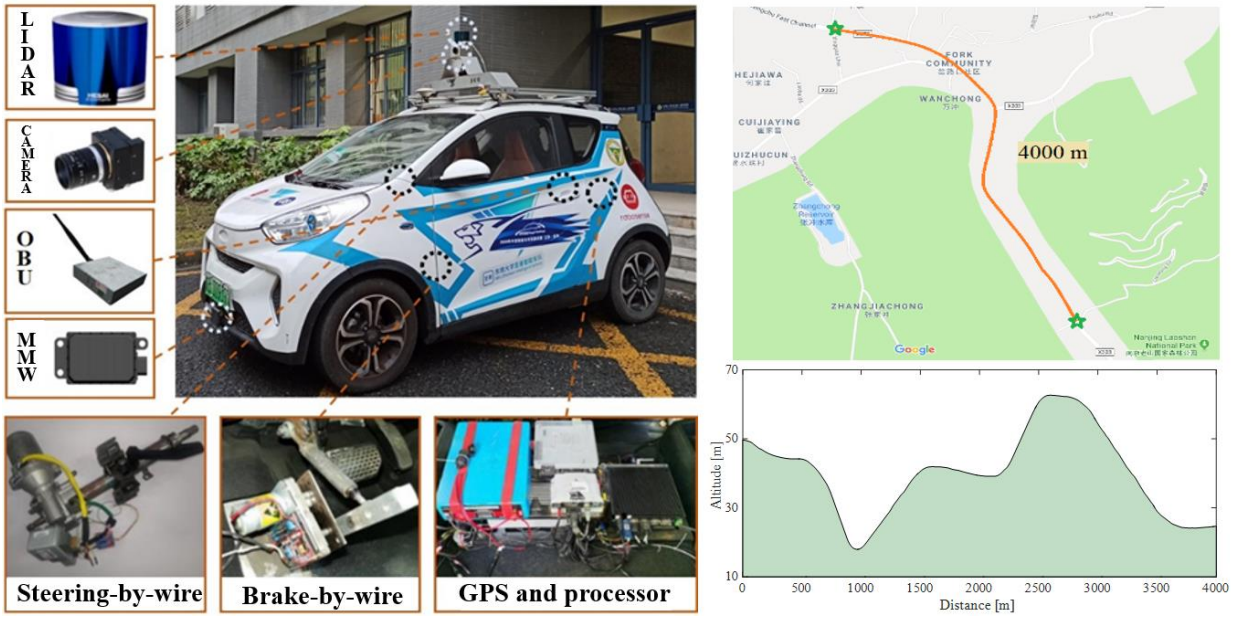


**Fig. 24.** Experimental platform and test road for connected and automated vehicle.

operate at a frequency of 10 Hz. This hierarchical control architecture ensures accurate control of the vehicle's dynamic behavior, thereby enhancing driving safety and performance to a significant extent.

In the vehicle-in-the-loop test, as shown in Fig. 24, a 4 km suburban highway near Laoshan in Nanjing is chosen. Note that the experiment is conducted between 4 a.m. and 5 a.m. on a certain morning. In situations with minimal to no other traffic participants and sufficient ambient light, which has a weaker impact on the energy-efficient driving of the host vehicle. Fig. 25 displays the velocity trajectory obtained by different driving strategies in the vehicle-in-the-loop test. The velocity trajectory of the NCMS exhibits a similar overall trend to that of IMPC. Nonetheless, the NCMS demonstrates markedly higher average velocities and a more pronounced velocity increment, corroborating the findings observed in the preceding virtual simulations. The NCMS demonstrates higher velocity, leading to increased energy consumption, as depicted in Table 6. Nonetheless, the energy consumption of NCMS is merely 2.82% higher than that of IMPC. Notably, NCMS achieves nearly 10 times the computational speed of IMPC when considering the single-step computation time based on the onboard vehicle controller. It is crucial to emphasize that the computation time mentioned in this context adheres to the real-time requirements of the proposed driving strategy. Moreover, the performance validation of NCMS and IMPC through vehicle-in-the-loop tests exhibits consistent trends with the simulation environment, providing further validation of the reliability of the simulation.

**Table 6**
Comparison of the results of NCMS and IMPC.

| Strategies | Energy consumption | Optimality | Calculation time per step |
|---|---|---|---|
| NCMS | 1668.9 kJ | -2.82% | 0.02 s |
| IMPC | 1623.6 kJ | | 0.26 s |

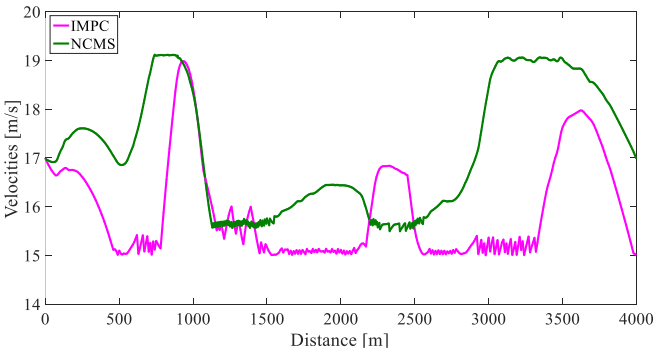


**Fig. 25.** Velocity trajectories by different driving strategies in the vehicle-in-the-loop test.

## 5. Conclusion

This paper proposes two real-time energy-oriented driving strategies, namely NCMS and IMPC. They are compared with DP and CS strategies in the simulation in terms of energy consumption and computational efficiency. The quantitative results demonstrate that the energy cost of the NCMS and IMPC can be saved by 8.23% and 11.64% respectively, when compared to the CS strategy, for 35 km of the experimental road. The latter is almost similar to the energy savings of the global optimal DP strategy. In addition, a vehicle-in-the-loop test demonstrates that the NCMS strategy is the most computationally efficient among all methods and maintains a good prospect of energy savings. The most important thing is that in order to ensure the real-time performance and safety of vehicles in real traffic conditions, a logic car-following algorithm is applied to NCMS with the expected results.

In the future, we will address the lateral planning and control of CEV for the eco-driving problem. Due to the complex and dynamic nature of real road environments, necessary lane changes are inevitable. Therefore, exploring how to enhance vehicle energy efficiency through both lateral and longitudinal movements will become a crucial research direction.

## Declaration of competing interest

The authors declare that they have no known competing financial interests or personal relationships that could have appeared to influence the work reported in this paper.

## Data availability

Data will be made available on request.

## Acknowledgements

This work is supported by the National Natural Science Foundation (NNSF) of China under Grants 52172383 and the Postgraduate Research & Practice Innovation Program of Jiangsu Province under Grant KYCX22_0196.

## References

[1] IEA. Tracking transport 2020. Paris: IEA; 2020. [Online]. Available:https://www.iea.org/reports/tracking-transport-2020.
[2] J.N. Barkenbus, Eco-driving: An overlooked climate change initiative. Energy Policy 38 (2010) 762-769, https://doi.org/10.1016/j.enpol.2009.10.021.
[3] B. Li, W. Zhuang and N. Chen, "Predictive Ecological Control: Using Road Terrain and Traffic Signal Information for Improving Vehicle Energy Efficiency, 2019 3rd Conference on Vehicle Control and Intelligence (CVCI), Hefei, China, (2019) 1-6, https://doi:10.1109/CVCI47823.2019.8951544.
[4] F. Li, L. Gao, Y. Zhang, Y. Liu, Hierarchical operation switch schedule algorithm for energy management strategy of hybrid electric vehicle using adaptive dynamic programming, Sustain. Energy Grids Netw. Available online (2023) 101107, https://doi.org/10.1016/j.segan.2023.101107.
[5] C. Chan, A. Bouscayrol, K. Chen, Electric, hybrid, and fuel cell vehicles: Architectures and modeling, IEEE Trans. Veh. Technol. 59 (2010) 589-598, https://doi.org/10.1109/TVT.2009.2033605.
[6] M. Hua, C. Zhang, F. Zhang, Z. Li, X. Yu, H. Xu, Q. Zhou. Energy management of multi-mode plug-in hybrid electric vehicle using multi-agent deep reinforcement learning. Applied Energy, 348 (2023) 121526, https://doi.org/10.1016/j.apenergy.2023.121526.
[7] J. Huang, Y. Kang, M. Liu, M. Cao, Q. Yan, Multi-Objective Optimization Control of Distributed Electric Drive Vehicles Based on Optimal Torque Distribution, IEEE Access 7 (2019) 16377-1639, https://doi.org/10.1109/ACCESS.2019.2894259.
[8] X. Sun, H. He, X. Liu, Motor fault tolerant control strategy for distributed driving electric vehicle, ITEC Asia-Pacific (2014) 1569951609, https://doi.org/10.1109/ITEC-AP.2014.6941121.
[9] M. Kamal, T. Hayakawa, and J. I. Imura, Development and evaluation of an adaptive traffic signal control scheme under a mixed-automated traffic scenario, IEEE Trans. Intell. Syst. 2 (2020) 590-602, https://doi.org/10.1109/TITS.2019.2896943
[10] J. Jin, X. Ma, A Multi-Objective Agent-Based Control Approach With Application in Intelligent Traffic Signal System, IEEE Trans. Intell. Syst. 20 (2019) 3900-3912, https://doi.org/10.1109/TITS.2019.2906260.

[11] L. Bai, J. Xu, Research on Urban Traffic Signal Control Method at Single Intersection, Adv. Mat. Res. 361 (2011) 1799-1802, https://doi.org/10.4028/www.scientific.net/AMR.361-363.

[12] M. Knowles, H. Scott, D. Baglee, The effect of driving style on electric vehicle performance, economy and perception, Int. J. Electric Hybrid Veh. vol. 4 (2012) 228-247, https://doi.org/10.1504/IJEHV.2012.050492.

[13] D. Lang, R. Schmied, L. Del Re, Prediction of preceding driver behavior for fuel efficient cooperative adaptive cruise control, SAE Int. J. Engines, 7 (2014) 14-20, https://doi.org/10.4271/2014-01-0298.

[14] B. Beusen, S. Broekx, T. Denys, Using on-board logging devices to study the longer-term impact of an eco-driving course, Transport. Res. D. 14 (2009) 514-520, https://doi.org/10.1016/j.trd.2009.05.009.

[15] L. He, T. Shen, L. Yu, N. Feng, J. Song, A model-predictivecontrol-based torque demand control approach for parallel hybrid powertrains, IEEE Trans. Veh. Technol. 62 (2013) 1041–1052, https://doi.org/10.1109/TVT.2012.2218291.

[16] H. K. Roy, A. McGordon, P. A. Jennings, A generalized powertrain design optimization methodology to reduce fuel economy variability in hybrid electric vehicles, IEEE Trans. Veh. Technol. 63 (2014) 1055-1070, https://doi.org/10.1109/TVT.2013.2283749.

[17] B. Yya, B. Hpa, C. Xhab, Fuel economy optimization of power split hybrid vehicles: A rapid dynamic programming approach, Energy, 166 (2019) 929-938, https://doi.org/10.1016/j.energy.2018.10.149.

[18] C. Zhai, F. Luo, Y. Liu. Cooperative Power Split Optimization for a Group of Intelligent Electric Vehicles Travelling on a Highway With Varying Slopes, IEEE Trans. Intell. Syst. 2 (2020) 91-103, https://doi.org/10.1109/TITS.2020.3045264.

[19] Y. Luo, K. Li, S. Li, Green light optimal speed advisory for hybrid electric vehicles, Mech. Syst. Signal Pr. 87 (2016) 30-44, https://doi.org/10.1016/j.ymssp.2016.04.016.

[20] S. Xu, S. E. Li, X. Zhang, Fuel-optimal cruising strategy for road vehicles with step-gear mechanical transmission, IEEE Trans. Intell. Syst. 16 (2015) 3496-3507, https://doi.org/10.1109/TITS.2015.2459722.

[21] M. A. S. Kamal, M. Mukai, J. Murata, Ecological vehicle control on roads with up-down slopes, IEEE Trans. Intell. Syst. 12 (2011) 783-794, https://doi.org/10.1109/TITS.2011.2112648.

[22] S. E. Li, H. Peng, K. Li, J. Wang. Minimum fuel control strategy in automated car-following scenarios, IEEE Trans. Veh. Technol. 61 (2012) 998-1007, https://doi.org/10.1109/TVT.2012.2183401.

[23] K. Luo, W. C. Zhuang, L. W. Xu, Energy-Efficient Feedback Control Strategy of Vehicle Platoon on Highway with Varying Slopes, Proc.CCC, Guangzhou, Guangdong, CA, (2019), https://doi.org/10.23919/ChiCC.2019.8865530.

[24] Z. Chen, C. C. Mi, J. Xu, X. Gong, C. You, Energy Management for a Power-Split Plug-in Hybrid Electric Vehicle Based on Dynamic Programming and Neural Networks, IEEE Trans. Veh. Technol. 63 (2014) 1567-1580, https://doi.org/10.1109/TVT.2013.2287102.

[25] J. Q. Wang, Q. W. Yu, S. B. Li, Economic speed optimization method based on real-time information of road slope, Journal of Automotive Safety and Energy Efficiency, 5 (2014). 257-262.

[26] W. Zhuang, Q. Linghu, S. Xv, Integrated energy-oriented cruising control of electric vehicle on highway with varying slopes considering battery aging, Sci. China Technol. Sci. 63 (2020) 155-165, https://doi.org/10.1007/s11431-019-9559-2.

[27] C. Sun, J. Leng, F. Sun, A Fast Optimal Speed Planning System in Arterial Roads for Intelligent and Connected Vehicles," IEEE Internet of Things Journal, 9 (2022) 20295-20307, https://doi.org/10.1109/JIOT.2022.3172009.

[28] H. Dong, W. Zhuang, H. Ding, Event-Driven Energy-Efficient Driving Control in Urban Traffic for Connected Electric Vehicles, IEEE Trans. Transp. Electrification, 9 (2023) 99-113, https://doi.org/10.1109/TTE.2022.3177466.

[29] C. Vagg, S. Akehurst, C. J. Brace, Stochastic dynamic programming in the real-world control of hybrid electric vehicles, IEEE Trans. Control Syst. Technol. 24 (2016) 853-866, https://doi.org/10.1109/TCST.2015.2498141.

[30] X. Hu, Y. Zou, Y. Yang, Greener plug-in hybrid electric vehicles incorporating renewable energy and rapid system optimization, Energy, 111 (2016) 971-980, https://doi.org/10.1016/j.energy.2016.06.037.

[31] G. R. Gonçalves da Silva, M. Lazar, Long hauling eco-driving: heavy-duty trucks operational modes control with integrated road slope preview, 2022 European Control Conference (ECC), London, United Kingdom, (2022) 1752-1758, https://doi.org/10.48550/arXiv.2203.12378.

[32] L. Guo, B. Gao, Y. Gao, H. Chen, Optimal Energy Management for HEVs in Eco-Driving Applications Using Bi-Level MPC, IEEE Trans. Intell. Transp. Syst. 18 (2017) 2153–2162, https://doi.org/10.1109/TITS.2016.2634019.

[33] Y. Zhang, Y. Huang, G. Li, An Optimal Control Strategy for Plug-In Hybrid Electric Vehicles Based on Enhanced Model Predictive Control With Efficient Numerical Method, IEEE Trans. Transp. Electrification, 8,(2022) 2516-2530, https://doi.org/10.1109/TTE.2022.3141191.

[34] B. Asadi, Vahidi, Predictive Cruise Control: Utilizing Upcoming Traffic Signal Information for Improving Fuel Economy and Reducing Trip Time, IEEE trans. control syst. Technol. 19 (2011) 707-714, https://doi.org/10.1109/TCST.2010.2047860.

[35] F. Ju, W. Zhuang, L. Wang, Iterative Dynamic Programming Based Model Predictive Control of Energy Efficient Cruising for Electric Vehicle with Terrain Preview, SAE Technical Paper, (2020). https://doi.org/10.4271/2020-01-0132.

[36] L. Guo, B. Gao, Y. Gao, H. Chen, Optimal energy management for HEVs in eco-driving applications using bi-level MPC, IEEE Trans. Intell. Transp. Syst. 18 (2016) 2153–2162. https://doi.org/10.1109/TITS.2016.2-634019.

[37] A.S.M. Bakibillah, M.A.S. Kamal, C.P. Tan, T. Hayakawa, Fuzzy-tuned model predictive control for dynamic eco-driving on hilly roads. Applied Soft Computing, 99 (2020) 106875. https://doi.org/10.1016/j.asoc.2020.-106875.

[38] A.S.M. Bakibillah, M.A.S. Kamal, C. Tan, T. Hayakawa, J. Imura, Ecodriving on hilly roads using model predictive control, IEEE Joint 7th International Conference on Informatics, Electronics & Vision (ICIEV) and 2nd International Conference on Imaging, Vision & Pattern Recognition, icIVPR, (2018) 476–480. https://doi.org/10.1109/ICIEV.2018.8640987.

[39] D. Jia, H. Chen, Z. Zheng, An Enhanced Predictive Cruise Control System Design With Data-Driven Traffic Prediction, IEEE Trans. Intell. Transp. Syst. 23 (2022) 8170-8183, https://doi.org/10.1109/TITS.2021.3076494.

[40] V. H. Johnson, Battery performance models in ADVISOR, J.Power Sources. 110 (2002) 321-329, https://doi.org/10.1016/S03787753-(02)00194-5.